Circulation: Arrhythmia and Electrophysiology

ORIGINAL ARTICLE

How Accurate Is Inverse Electrocardiographic Mapping?

A Systematic In Vivo Evaluation

Laura R. Bear, PhD
Ian J. LeGrice, MBChB, PhD
Gregory B. Sands, PhD
Nigel A. Lever, MBChB, FRACP
Denis S. Loiselle, PhD
David J. Paterson, DSc
Leo K. Cheng, PhD
Bruce H. Smaill, PhD

BACKGROUND: Inverse electrocardiographic mapping reconstructs cardiac electrical activity from recorded body surface potentials. This noninvasive technique has been used to identify potential ablation targets. Despite this, there has been little systematic evaluation of its reliability.

METHODS: Torso and ventricular epicardial potentials were recorded simultaneously in anesthetized, closed-chest pigs (n=5), during sinus rhythm, epicardial, and endocardial ventricular pacing (70 records in total). Body surface and cardiac electrode positions were determined and registered using magnetic resonance imaging. Epicardial potentials were reconstructed during ventricular activation using experiment-specific magnetic resonance imaging–based thorax models, with homogeneous or inhomogeneous (lungs, skeletal muscle, fat) electrical properties. Coupled finite/boundary element methods and a meshless approach based on the method of fundamental solutions were compared. Inverse mapping underestimated epicardial potentials >2-fold (P<0.0001).

RESULTS: Mean correlation coefficients for reconstructed epicardial potential distributions ranged from 0.60±0.08 to 0.64±0.07 across all methods. Epicardial electrograms were recovered with reasonable fidelity at ≈50% of sites (median correlation coefficient, 0.69–0.72), but variation was substantial. General activation spread was reproduced (median correlation coefficient, 0.72–0.78 for activation time maps after spatio-temporal smoothing). Epicardial foci were identified with a median location error ≈16 mm (interquartile range, 9–29 mm). Inverse mapping with meshless method of fundamental solutions was better than with finite/boundary element methods, and the latter were not improved by inclusion of inhomogeneous torso electrical properties.

CONCLUSIONS: Inverse potential mapping provides useful information on the origin and spread of epicardial activation. However the spatio-temporal variability of recovered electrograms limit resolution and must constrain the accuracy with which arrhythmia circuits can be identified independently using this approach.

Key Words: arrhythmias, cardiac ■ electrocardiography ■ epicardial mapping ■ magnetic resonance imaging ■ torso

http://circep.ahajournals.org

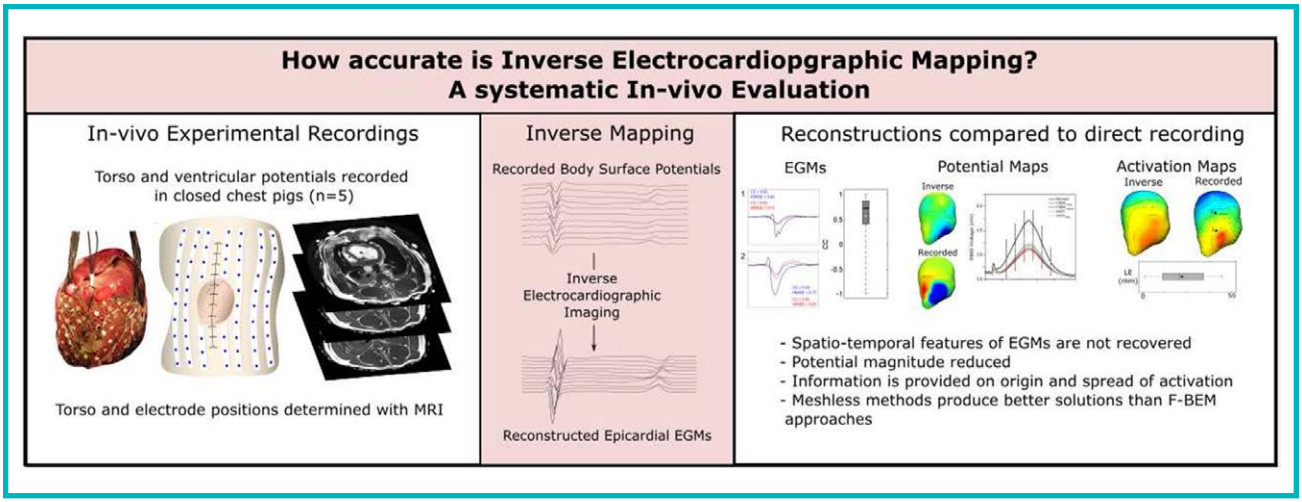

WHAT IS KNOWN?

- Noninvasive electrocardiographic imaging has the potential to complement conventional methods by providing information on cardiac electrical activity that cannot be obtained with intracardiac catheters alone.
- There have been few attempts to validate electrocardiographic imaging methods by direct comparison of estimated and recorded epicardial potentials.

WHAT THE STUDY ADDS?

- We have completed a systematic investigation of how faithfully electrograms across the epicardial surface of the ventricles are recovered with electrocardiographic imaging using a porcine experimental model.
- Recovered epicardial electrograms were substantially lower in magnitude than recorded, and key spatio-temporal features were not reproduced.
- Inverse potential mapping provides qualitative information on the origin and spread of epicardial activation, but spatial resolution is poorer than has previously been claimed.

It is necessary to identify cardiac regions that trigger focal activation and provide substrates for reentrant arrhythmias to ablate them effectively. Although intracardiac electroanatomic mapping is widely used for this purpose,[1] epicardial electrical activity can also be reconstructed noninvasively from body surface potentials using inverse mapping methods.[2] This approach is also referred to as electrocardiographic imaging (ECGi). It has been used to map electrical activity in ventricular tachycardia,[3–5] persistent atrial fibrillation,[6–8] and to help identify responders in cardiac resynchronization therapy.[9,10] Inverse mapping could also complement conventional methods, providing information on epicardial exit sites and potential intramural reentrant pathways that cannot be obtained with intracardiac catheters alone.[5,6]

Noninvasive imaging of epicardial potentials from body surface measurements requires the solution of Laplace equation in the volume between the epicardial surface of the heart and torso surface.[2] The problem is simplified if this domain is treated as a uniform isotropic volume conductor, an assumption made in most inverse mapping tools in clinical use.[3–10] This is justified, in part, by the accuracy of the approach in laboratory studies where dog hearts were suspended in an electrolyte-filled tank shaped like a human torso[11,12] and by computational analyses that show that incorporation of more realistic inhomogeneous torso electrical properties may not lead to more accurate solutions of the inverse problem in the presence of electrical noise or measurement uncertainty.[13]

Despite increasing clinical use of ECGi, there have been surprisingly few attempts to evaluate inverse potential mapping methods by comparing estimated and recorded epicardial potentials directly in appropriate in vivo experimental models. Localization errors (LEs) for known cardiac pacing sites in studies with human subjects[4–6,14–17] have ranged from 6 to 50 mm. Studies in dogs showed that inverse mapping captures the general spread of epicardial activation[18,19] and, in the most recent of these,[19] known pacing sites were identified with a median error of 10 mm for a range 4 to 45 mm. However, in this latter work, epicardial recordings were acquired at the apex and superior surface of the ventricles while pacing was applied at these sites only.

The objective of this study was to complete a systematic evaluation of the accuracy of inverse epicardial potential mapping. To this end, we have established an experimental framework that encompasses simultaneously recorded body surface and epicardial potentials for a wide range of stimulus sites. These data are associated with experiment-specific reconstructions

of 3-dimensional (3D) torso anatomy, as well as the locations of recording and pacing electrodes. This has enabled systematic comparison of measured epicardial potentials with potential distributions reconstructed using well-established inverse methods. ECGi methods comparable to those used clinically were evaluated in this study, including those that incorporate more realistic torso electrical properties.

METHODS

A subset of the experimental data acquired in this study have been made available for the electrocardiographic imaging community, through the EDGAR project (Experimental Data and Geometric Analysis Repository; http://www.ecg-imaging.org/),[20] a collaborative effort by the Consortium for ECG Imaging. The analytic methods used are not included because there are open-source applications that are already widely available.

Experimental Procedures

The experimental methods used here have previously been described[21] and are summarized below. All surgical procedures were approved by the Animal Ethics Committee of the University of Auckland and conform to the Guide for the Care and Use of Laboratory Animals (National Institutes of Health publication no. 85-23).

Electrical mapping was performed in 5 anesthetized, closed-chest, pigs (30–40 kg). The heart was exposed via a midline sternotomy and supported in a pericardial cradle. A custom-made elastic sock containing 239 unipolar silver electrodes (≈1.5 mm diameter, 5–10 mm spacing) was drawn over the ventricles. The thorax was closed and air expelled. Flexible strips (BioSemi, the Netherlands) containing 184 electrodes (30–45 mm spacing) were attached to the body surface. Epicardial and body surface potentials were recorded simultaneously using separate acquisition systems (UnEmap, Auckland Uniservices, New Zealand; ActiveTwo, BioSemi). For both, signals were referenced to adjacent common electrodes on the lower abdomen and were bandlimited (0.05–1000 Hz) and sampled at 2 kHz. For each pig, recordings were made during (1) sinus rhythm (n=1), (2) pacing from left and right ventricular endocardium (n=3–12), and epicardium (n=4–16). Overall, 70 records were obtained. On completion of each experiment, the heart was arrested with potassium citrate, and magnetic resonance (MR) images of the heart and thorax were acquired. The heart was then excised and perfusion-fixed with 3% formalin in phosphate buffer. Epicardial electrode locations were captured with a multiaxis digitizing arm (FARO Technologies, FL). MR imaging contrast markers placed on the sock and body surface strips were localized in the MR images and used to register electrode locations.

Inverse Mapping Methods

Two different inverse mapping approaches were used: coupled finite/boundary element methods (F-BEM),[22,23] which enable electrical properties to be defined in specified torso regions, and a meshless method of fundamental solutions (mMFS) approach.[24] The F-BEM models were customized from experiment-specific MR images for each animal using (1) homogeneous conductivity between heart and body surface (F-BEM$_{homog}$), and (2) inhomogeneous conductivity (F-BEM$_{inhomog}$) in which separate electrical properties were assigned to the lungs, fat, torso cavity (assumed isotropic), and skeletal muscle (assumed anisotropic). Parameters and further details of the 2 volume conductor models are presented in the Data Supplement for Bear et al.[21] With mMFS, the torso is assumed to be a homogeneous volume conductor. For the F-BEM models, Kriging interpolation was used to map potentials from the body surface electrodes onto the torso. To ensure that any differences between F-BEM and mMFS were not because of the interpolation, interpolated torso potentials were also used as the inputs for an mMFS inverse solution. These 2 cases are identified as mMFS and mMFS$_{interp}$, respectively.

For each of these models, recorded body surface potentials were used to reconstruct potentials at 622 sites on the ventricular epicardium using Tikhonov regularization[25] and CRESO criteria (Composite Residual and Smoothing Operator).[26]

Data Analysis

Instantaneous epicardial potential distributions were reconstructed from recorded body surface recordings, and data analysis was performed on 1 representative ventricular activation complex for each record. Reconstructed potentials were interpolated on the epicardial surface to enable direct comparison with recorded cardiac potentials. Activation times (ATs) for measured and reconstructed epicardial electrograms were estimated from the maximum negative potential derivative. Global activation fields were also fitted to these estimates to produce more spatially coherent activation maps.[27]

Correspondence between measured and reconstructed AT maps and epicardial potential distributions at each point in time were quantified by evaluating root-mean-squared (RMS) voltage, relative RMS error (rRMSE), and the correlation coefficient (CC).

$$\text{RMS Voltage} = \frac{\sqrt{\sum_{i=1}^{N}\left(X^i_{M\,or\,R}\right)^2}}{N} \quad (1)$$

$$\text{rRMSE} = \sqrt{\frac{\sum_{i=1}^{N}\left(X^i_M - X^i_R\right)^2}{\sum_{i=1}^{N}\left(X^i_M\right)^2}} \quad (2)$$

$$\text{CC} = \frac{\sum_{i=1}^{N}\left(X^i_M - \mu_M\right)\left(X^i_R - \mu_R\right)}{\sqrt{\sum_{i=1}^{N}\left(X^i_M - \mu_M\right)^2}\sqrt{\sum_{i=1}^{N}\left(X^i_R - \mu_R\right)^2}} \quad (3)$$

where N is the number of epicardial electrodes, X^i_M and X^i_S are the potential or AT at electrode i for measured (M) and reconstructed (R) data while μ_M and μ_S are corresponding mean values across all electrodes.

The temporal correspondence of measured and reconstructed epicardial electrograms was also compared by evaluating rRMSE and CC at individual electrodes. Here, i and N in Equations 1 to 3 are time and number of samples, respectively, and μ_M and μ_S in this case are mean values of measured and reconstructed epicardial electrograms across the ventricular activation sequence.

LE was estimated as the Euclidean distance between measured and reconstructed locations of the site of earliest activation.

Because calculated LEs were non-normally distributed in every case and because the CC is inherently non-normally distributed, we analyzed the LE data as well as CCs for epicardial electrograms and AT maps using the NPAR1WAY module available in the Statistical Analysis System software package. The statistical significance of differences among medians was sought using its MEDIAN function, adopting a value of α (the probability of a type I error) of 0.05. AT map CCs and LEs, estimated from the maximum negative potential derivative for all 70 recordings, were compared with equivalent results generated after additional smoothing. Examination of differences among subsets of these data (anterior versus posterior and base-mid-apex) were performed with the smoothed data only.

RESULTS

Comparison of Recorded and Reconstructed Epicardial Potential Distributions

Figure 1 illustrates the reconstructed epicardial potential distributions for a representative study during epicardial pacing from the anterior right ventricle free wall. The figure compares anterior views at 3 representative times during ventricular activation of measured body surface potentials with epicardial potentials reconstructed from them using F-BEM$_{homog}$, F-BEM$_{inhomog}$, and mMFS inverse solutions. (Corresponding results for mMFS$_{interp}$ are not presented because in this case they are indistinguishable from mMFS.) There is qualitative correspondence in the spatio-temporal progression of measured and reconstructed potential distributions. Epicardial depolarization occurs first in the right ventricle and then spreads leftward reflecting the changing distribution of body surface potentials. However, there are clear differences between reconstructed and measured epicardial potentials. Early right ventricle depolarization in the region surrounding the pacing electrode is not captured in any of the reconstructions. The rapid spatial variation in potential adjacent to the wavefront of depolarization is not replicated. Finally, the magnitudes of reconstructed epicardial potentials are substantially underestimated.

The correspondence between recorded and reconstructed epicardial potentials was gauged by evaluating RMS voltage and CC across all 239 epicardial sites at successive instants during ventricular activation. Results averaged across the complete data set are shown in Figure 2. Potentials reconstructed across the epicardial surface substantially underestimate the magnitude of measured potentials throughout activation although on average the timing of activation is recovered relatively well. CCs are low initially during activation but rise to ≈0.6 subsequently, indicating a moderate correspondence between measured and reconstructed epicardial

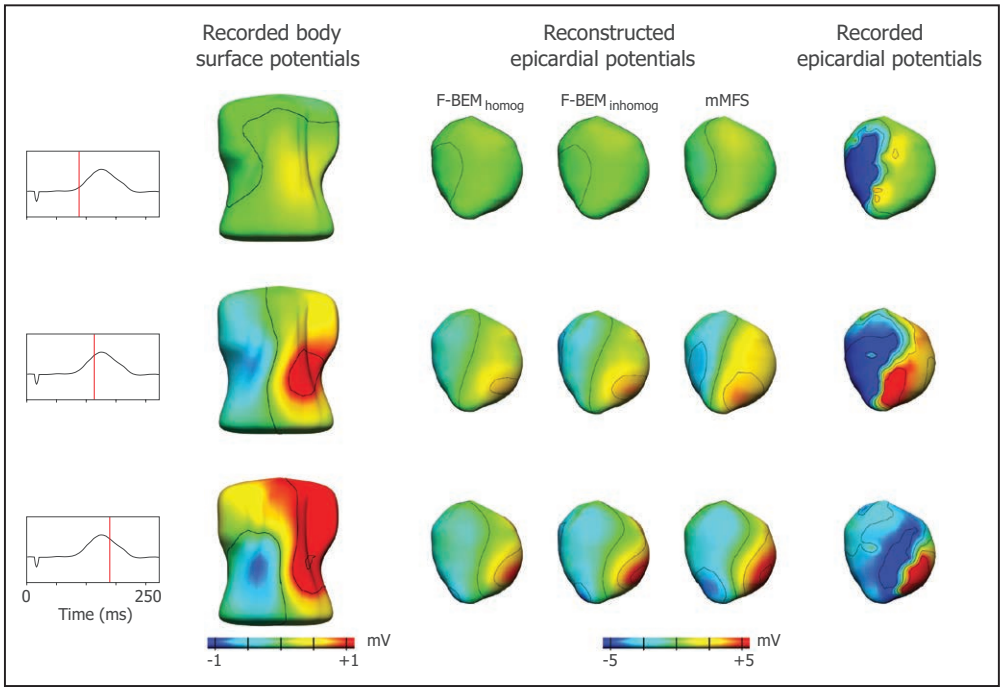

Figure 1. Validation of inverse electrocardiographic mapping: ventricular epicardial potentials are reconstructed from measured body surface potentials.

A coupled finite/boundary element approach using homogeneous and inhomogeneous forward models (finite-boundary element method [F-BEM]$_{homog}$ and F-BEM$_{inhomog}$, respectively) is used, as well as a meshless method using the method of fundamental solutions (mMFS). The inverse solutions obtained are compared with potentials measured simultaneously on the ventricular epicardial surface. Snapshots are presented at 3 instants during ventricular activation for a representative study in which epicardial pacing from the anterior right ventricle free wall.

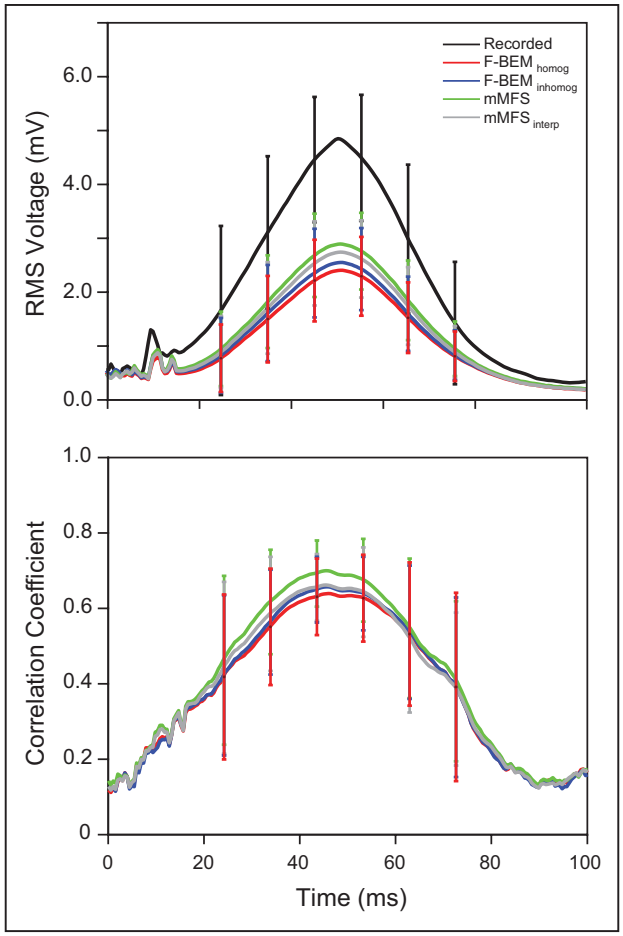

Figure 2. Comparisons of recorded and reconstructed epicardial potential distributions as a function of time during ventricular activation. Mean±SD across epicardial sites for all 70 records are presented at successive instants during activation. **A**, Root-mean-squared (RMS) voltages for recorded epicardial potentials (black) and epicardial potentials reconstructed using finite-boundary element method (F-BEM)$_{homog}$ (red), F-BEM$_{inhomog}$ (blue), meshless method of fundamental solutions (mMFS; green), and mMFS$_{interp}$ (gray) inverse solutions. **B**, Correlation coefficients (CCs) for recorded epicardial potentials distributions and distributions reconstructed using F-BEM$_{homog}$ (red), F-BEM$_{inhomog}$ (blue), mMFS (green), and mMFS$_{interp}$ (gray) inverse solutions.

potential distributions during much of the activation period.

For each activation sequence, RMS voltage and CC were averaged over the interval during which CC was ≥0.5 and stable. A summary of the results is presented in Table 1. Reconstructed epicardial RMS voltages were substantially smaller than recorded (P<0.0001) for all activation sequences with all inverse methods. There were small differences in mean RMS voltage for the 4 inverse solution methods with mMFS consistently greater than F-BEM (P<0.0001). However, there was no significant difference between F-BEM$_{homog}$ and F-BEM$_{inhomog}$ or between mMFS and mMFS$_{interp}$. There were also small differences in CC for the 4 inverse methods tested (0.60–0.64, respectively). Although the improvement was marginal, mMFS was significantly better than both F-BEM models (P<0.0001) and mMFS$_{interp}$ was better than mMFS (P<0.01). There was no difference between F-BEM$_{homog}$ and F-BEM$_{inhomog}$.

Table 1. Summary of RMS$_V$ and CC Used to Compare Reconstructed and Recorded Potential Maps for All Animals

		Inverse			
	Recorded	F-BEM$_{homog}$	F-BEM$_{inhomog}$	mMFS	mMFS$_{interp}$
RMS$_V$*,†	4.47±1.03	1.81±0.51	1.91±0.56	2.19±0.45	2.07±0.46
CC†,‡	…	0.60±0.08	0.61±0.07	0.61±0.07	0.64±0.07

Results presented as mean±SD of pooled data. CC indicates correlation coefficient; F-BEM, finite-boundary element method; mMFS, meshless method of fundamental solutions; and RMS$_V$, relative root-mean-squared error.
*Significant difference between measured and reconstructed values.
†Between reconstructed values using F-BEM and mMFS.
‡Between the interpolated and standard mMFS.

Reconstruction of Epicardial Potentials

In Figure 3, measured and reconstructed epicardial electrograms are presented at representative sites during ventricular activation for the study presented in Figure 1. Here also, results for mMFS$_{interp}$ are not included because the electrograms with both mMFS approaches are similar in this case. The magnitudes of reconstructed electrograms are substantially smaller than recorded. Although gross topology is generally captured, complex waveforms are poorly reproduced, and the intrinsic deflection is often temporally shifted with respect to the recorded epicardial electrograms.

CCs for measured and reconstructed electrograms were estimated at each epicardial electrode across the data set, and results are given in Figure 4. These data are presented as box plots because CC varies between ±1 and was not normally distributed across this range. Figure 4A shows CC distributions for each of the 4 inverse methods across all electrodes for the 70 records analyzed (N=15917). Median CC between measured and recovered epicardial electrograms was ≈0.7, but interquartile ranges were wide. That is, while correspondence was reasonable in ≈50% of cases, it was much less good in the remainder. There was no significant difference between methods and, in Figure 4B, CCs are compared by epicardial region for mMFS alone. Median CC was significantly greater for anterior than posterior sites (0.76 versus 0.68; P<0.001) and increased progressively from apex to base (P<0.01). These trends were replicated across epicardial regions for all methods and all stimulus types.

The correspondence between measured and reconstructed electrograms was also gauged by estimating rRMSE. Mean rRMSE ranged from 0.83±0.09 to 0.87±0.07 for the 4 inverse methods across the complete data set. With this index, mMFS was significantly better than F-BEM (P<0.0001) although the extent of this improvement was marginal. There was no dif-

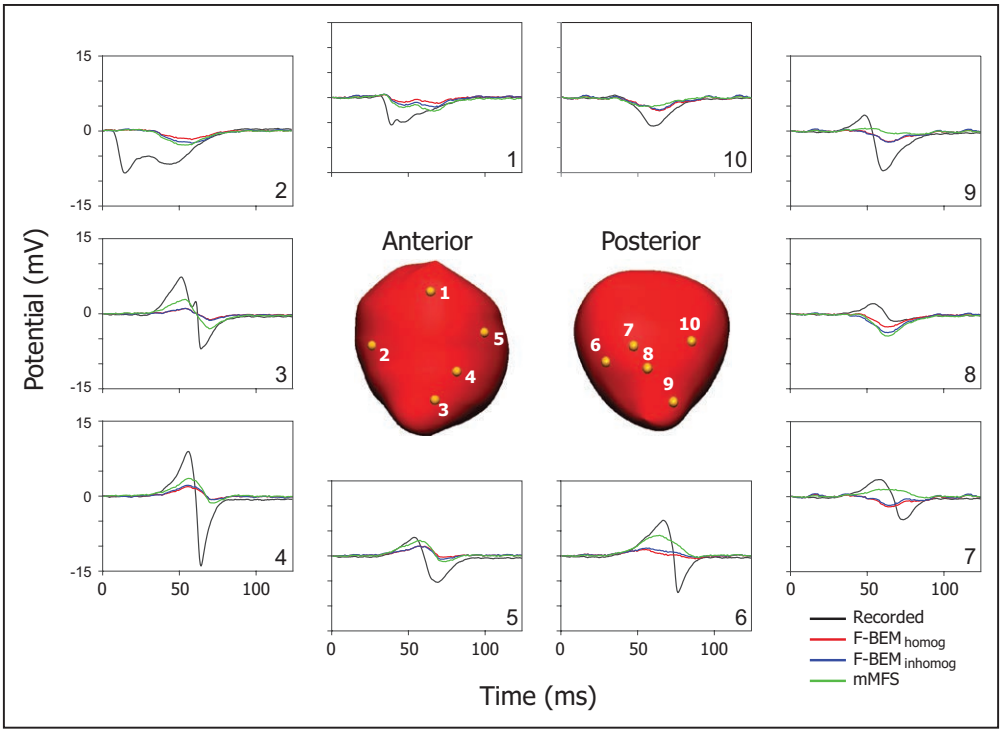

Figure 3. Ventricular electrograms recorded at selected epicardial sites for representative study compared with electrograms reconstructed at those sites using finite-boundary element method (F-BEM)$_{homog}$, F-BEM$_{inhomog}$, and meshless method of fundamental solutions (mMFS) inverse solutions.
Data from study in Figure 1, with epicardial pacing from the anterior right ventricle free wall.

ference between standard and interpolated mMFS approaches or between F-BEM$_{homog}$ and F-BEM$_{inhomog}$. Across all methods, rRMSE was >0.6 in >75% of cases. In part, this can be explained by the difference in amplitudes of measured and reconstructed epicardial electrograms (see Table 1). However, rRMSE is greater in general than can be explained on this basis alone.

Taken together, the results for CC and rRMSE demonstrate that although inverse methods often captured the general shape of measured electrograms, fine detail and accurate timing of the principal deflections were not well reproduced.

Comparison of Recorded and Reconstructed Epicardial AT Maps

AT maps were computed by fitting smoothed activation fields for all electrograms, and the additional smoothing improved correspondence between recorded and reconstructed AT maps. Over all 70 records, median CC was 0.66 to 0.69 across inverse methods using the derivative method alone but increased to 0.73 to 0.78 after spatial AT smoothing. This regularization increased CC for all methods (P<0.001), and the improvement was greatest with mMFS$_{interp}$ (P<0.03). Likewise, LE was also reduced for all inverse methods after smoothing and was significantly better with mMFS$_{interp}$ than F-BEM (P<0.0001).

In Figure 5, we present smoothed AT maps estimated from recorded electrograms as well as from electrograms reconstructed in a representative study using the best-case mMFS$_{interp}$ method. Here, anterior midbasal epicardial stimulation was applied, and correspondence between measured and reconstructed activation spread is good (CC=0.82 and LE=9.43 mm). However, there is evident truncation of the AT range in the inverse map.

Distributions of CC with mMFS$_{interp}$ for the complete data set are shown in Figure 6A before and after AT smoothing. CCs after smoothing are also presented for epicardial stimuli alone and by epicardial stimulus region. Smoothing increased median CC from 0.69 to 0.78 overall (P<0.001), but there was no significant difference between results with epicardial stimulation or from different epicardial stimulus regions. Comparable data for LE are presented in Figure 6B although epicardial breakthrough sites in sinus rhythm were not included. Median LE was reduced from 20.2 to 15.75 mm by AT map smoothing (P<0.05), but the variation in LE was substantial with an interquartile range of 9 to 29 mm. There was no significant difference with epicardial stimulation only or for epicardial stimulation in different regions. Similar results were obtained when these AT analyses were applied with different inverse solution methods.

DISCUSSION

The clinical use of noninvasive electrocardiographic mapping has attracted considerable recent interest.[2–10]

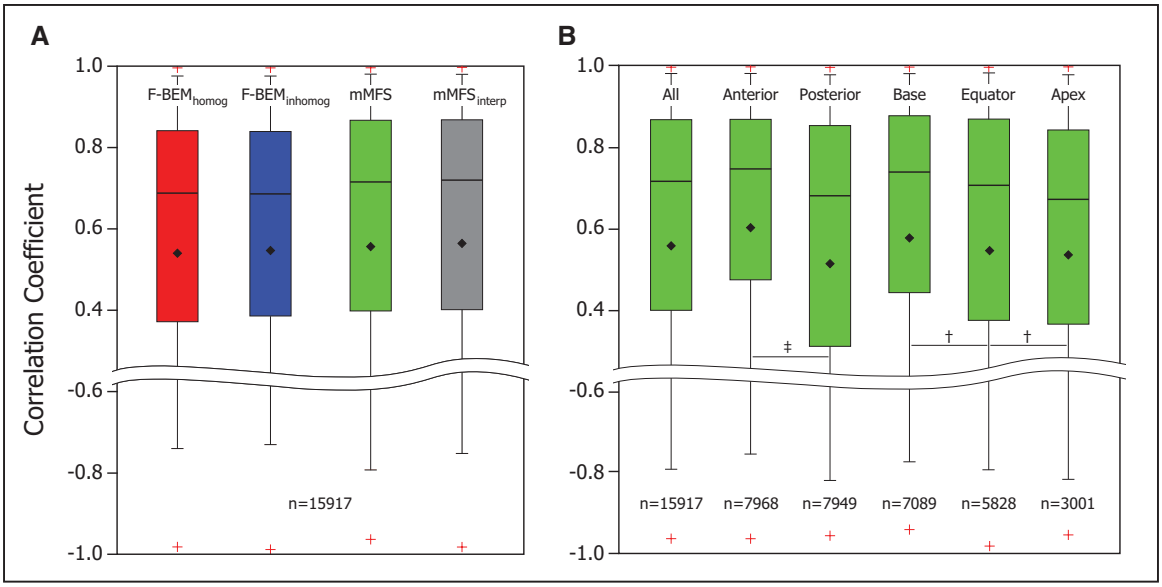

Figure 4. Boxplots of correlation coefficients (CC) showing recorded and reconstructed epicardial electrograms across epicardial recording sites. The thick lines represent the medians, the diamonds the means, the boxes the interquartile range, the whiskers the 1st and 99th percentiles, and the red crosses the maximum and minimum values. The number of electrograms compared is given in each case. **A**, CCs for 4 inverse methods across all 70 records. **B**, CCs for meshless method of fundamental solutions (mMFS) inverse method by epicardial region. These include anterior and posterior epicardium and basal, equatorial, and apical regions across both. Probabilities that distributions are significantly different: †$P \leq 0.01$ and ‡$P \leq 0.001$. F-BEM indicates finite-boundary element method.

Inverse potential mapping in human subjects recovers epicardial activation patterns in normal rhythm and across a wide range of heart rhythm disturbances that conform with expectations based on anatomy, physiology, and pathophysiology. For example, inverse methods have been used to identify the origin of premature ventricular complexes and to map reentrant circuits in ventricular arrhythmia.[5] It has also been demonstrated that epicardial potentials and activation mapped in patients with healed myocardial infarction are consistent with scar geometry reconstructed with magnetic resonance and computed tomographic imaging[26] and that inverse mapping captures characteristic features of ventricular electric dyssynchrony in heart failure.[9,10] Finally, epicardial resolution better than 10 mm is widely claimed for this approach.[5,9,11–14]

We demonstrate that although inverse electrocardiographic mapping substantially underestimated epicardial potential magnitudes, general features of activation spread could be recovered with reasonable accuracy. The mMFS performed better than F-BEM across several correspondence measures. However, in our hands, sites of epicardial breakthrough and stimulation were recovered with less precision than has been reported elsewhere.[5,11,12]

Comparison With Previous Findings

Rudy and coworkers completed systematic experimental studies with perfused dog hearts suspended in a child-sized torso-shaped tank filled with saline, in which epicardial and torso surface potentials were recorded simultaneously.[11,12] Epicardial electrograms were reconstructed from recorded tank surface potentials over a wide range of conditions using inverse methods that represented the tank as a uniform isotropic volume conductor. Epicardial potentials were faithfully recovered (CC >0.9 for 72% of electrodes), and pacing sites were located within 2 to 10 mm.[11] Similar performance is claimed for the Medtonic CardioInsight mapping system, which specifies 6.8±2 mm resolution for 3D maps of epicardial electrical activation.

The accuracy with which initiation induced by pacing or ectopic foci can be identified with ECGi has been assessed in human studies by comparing inverse maps with electroanatomic maps acquired invasively at the same time or with pacing catheter locations estimated directly via 3D imaging. Rudy states that initiation sites (induced by pacing electrodes identified with computed tomography) were located noninvasively using ECGi with a spatial accuracy on the order of 6 mm.[2] Revishvili et al[17] found that atrial and ventricular endocardial pacing locations could be identified to within 7±2 mm relative to corresponding electroanatomic maps in 5 patients, but reported LEs of 9±6 mm in 26 patients when the 3D locations of endocardial pacing wires were quantified directly with MR imaging. Finally, Bhagirath et al[16] compared estimated endocardial locations of ventricular ectopic foci targeted for ablation with epicardial activation sites identified using inverse mapping with homogeneous and inhomogeneous torso models. They reported LEs of 10±3 and 8±3 mm, respectively, in 8 patients. Such studies indicate that inverse potential mapping can provide clinically useful information about epicardial electrical activation. However, they remain qualitative in that endocardial sites identified with varying levels of resolution were related to epicardial measures while

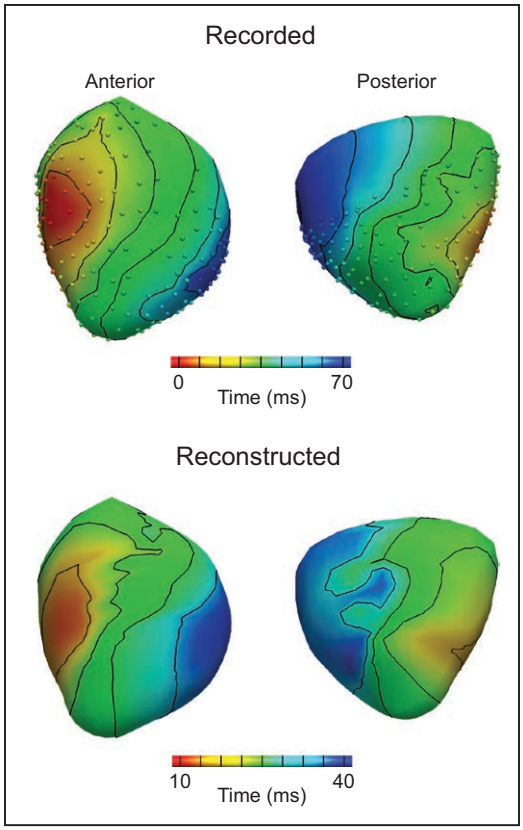

Figure 5. Anterior and posterior views of smoothed activation time map estimated from recorded epicardial electrograms compared with corresponding map determined from epicardial electrograms reconstructed using an meshless method of fundamental solutions $(mMFS)_{interp}$ inverse solution.
Data from representative study with midbasal epicardial stimulation applied on the anterior right ventricle free wall.

systematic comparisons with measured epicardial potentials or measures derived from them were not made. Furthermore, the assessments were not unblinded in a strict sense. Direct comparisons between inverse potential mapping and recorded epicardial potentials have also been made in human studies in which torso anatomy was extracted from computed tomographic images, and electrical properties were assumed to be homogeneous.[4,5,14] The first study was performed on 3 subjects during intrathoracic surgery.[14] Ventricular epicardial electrograms acquired with multielectrode patches were compared with electrograms reconstructed from body surface potential maps recorded before or after surgery. Time delays between reconstructed and recorded electrograms were variable while amplitudes were markedly different. However, morphology was predicted with reasonable fidelity at many sites (CC_{mean} ≈0.70±0.23), and initial activation was localized to 13±8 mm. A complementary study was also completed in 4 patients undergoing percutaneous epicardial catheter mapping before ablation of ventricular tachycardia.[4] Body surface potential maps were recorded in sinus rhythm and during pacing from multiple epicardial sites. Activation maps derived from reconstructed epicardial potentials were qualitatively similar to those assembled from point-by-point intrapericardial contact recordings. Localization of epicardial pacing sites and initial activation ranged from 13±9 mm over normal myocardium to 50±47 mm at the margin of myocardial infarct scar.

The only previous large animal study directly comparable to ours was performed recently by Cluitmans et al[19] in dogs using homogeneous computed tomography–based torso models. A difference in approaches is that we recorded electrograms at 239 electrodes distributed uniformly across the ventricular epicardial surface, whereas they used 103 nonuniformly spaced electrodes concentrated in basal and midbasal regions. We were, therefore, able to record epicardial potentials across the full epicardial surface and apply stimulation from a wider range of epicardial sites. Although our validation is based on a more varied experimental data set, our findings match in many respects. In particular, CC distributions for measured and reconstructed epicardial electrograms for both studies coincide almost exactly. However, estimates of LE differ. Cluitmans et al[19] report greater LE variability when AT maps are based on derivative measures only (median 33 mm, interquartile range, 23–44 mm) but less after spatio-temporal smoothing of AT maps (median, 10 mm; interquartile range, 7–17 mm).

Table 2 summarizes the results of studies in which inverse potential mapping was validated by direct comparison with recorded epicardial potentials. It is noteworthy that electrogram CC are consistently worse with human studies and animal experiments than in the smaller number of investigations using the torso tank. Furthermore, mean and median LEs range from 10 to 16 mm in the former studies compared with 2 to 10 mm in the torso tank.

Sources of Error With Inverse Mapping

Torso tank experiments[11,12] demonstrate the accuracy that can be achieved with inverse potential mapping when the forward problem is accurately formulated. The relationship between potentials on heart and torso surface can be specified with accuracy and relative simplicity because the tank is filled with saline, which has uniform isotropic electrical properties. This is not the case for the torso in vivo. However, computational analyses have demonstrated that torso models that incorporate more realistic electrical properties do not improve inverse solutions in the presence of electrical noise or geometric measurement error.[28,29] This has strengthened a view that inverse mapping can be used to recover epicardial electrical activity with an accuracy comparable to that achieved in torso tank.

That view is not supported by our results or those of other comparable validation studies (see Table 2). Inhomogeneous torso models produced no systematic

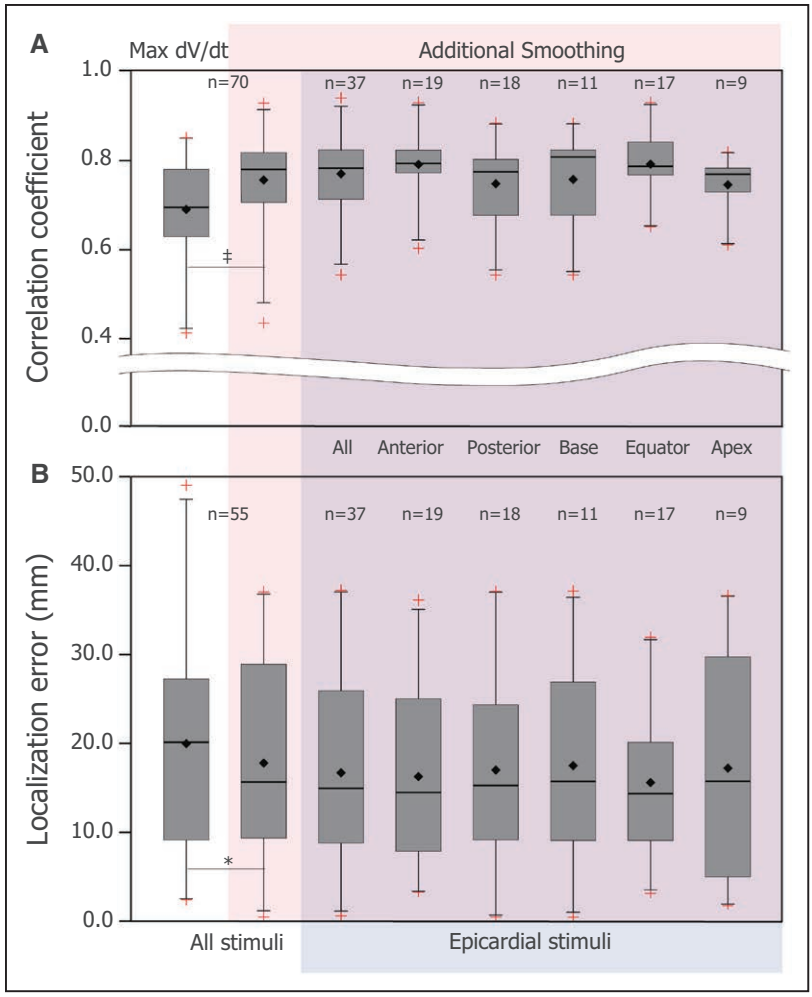

Figure 6. Correspondence between epicardial activation time (AT) maps estimated for recorded and reconstructed electrograms and initial activation sites derived from them.
Data in the leftmost panel relate to AT maps estimated using derivative method only while in all other cases, additional spatio-temporal smoothing is applied. The color-coded rightmost panel presents results for epicardial stimulation only, and results for different stimulus region are presented. Distributions are represented as boxplots; The thick lines represent the medians, the diamonds the mean values, the boxes the interquartile range, the whiskers the 1st and 99th percentiles, and the red crosses the maximum and minimum values. The number of electrograms considered is given in each case. Probabilities that distributions are significantly different: *$P \leq 0.05$ and ‡$P \leq 0.001$. **A**, Correlation coefficients (CC) for meshless method of fundamental solutions (mMFS) inverse method for all records including sinus rhythm (SR). **B**, Differences between sites of initiation identified in measured and reconstructed epicardial AT maps. Localization errors for SR are not included.

improvement over homogeneous models here, but the fidelity of the epicardial electrograms recovered with all inverse mapping methods was significantly poorer than is reported for torso tank studies. CC was >0.7 in ≈50% of cases only and varied widely within individual activation sequences. Reflecting this mean and median LEs tabulated in Figure 7 are in the range 10 to 15 mm, and most exhibit wide variability.

Much of this error is likely because of the fact that inverse solutions are inherently unstable, and this is exacerbated by noise in measured potentials and errors in the formulation of the forward problem. For example, the complex relative motion of heart and body surface that occurs with respiration is not captured in the static computed tomography or MR imaging–based torso models used in inverse mapping. This introduces geometric error in the forward problem that may be compounded in the inverse solution. Therefore, although torso tank experiments can be used to demonstrate the efficacy of inverse mapping methods, the accuracy

Table 2. Comparison of Previous Inverse Epicardial Potential Mapping Validation Studies in Ventricles

	Subjects	Cycles	Electrogram Correlation	Localization Error, mm	Activation Time Correlation	References
Torso tank		4	>0.8	2–10		11,12
Human	3	5	0.72±0.25	13±8		14
	4	79		13±9		4
Dog	4	93	0.71 [0.36–0.86]	10 [7–17]	0.82	19
Pig	5	70	0.72 [0.40–0.84]	16 [9–29]	0.78	This study

Numbers of individual studies and total activation cycles analyzed are indicated. Results are presented as mean±SD or median and [interquartile range].

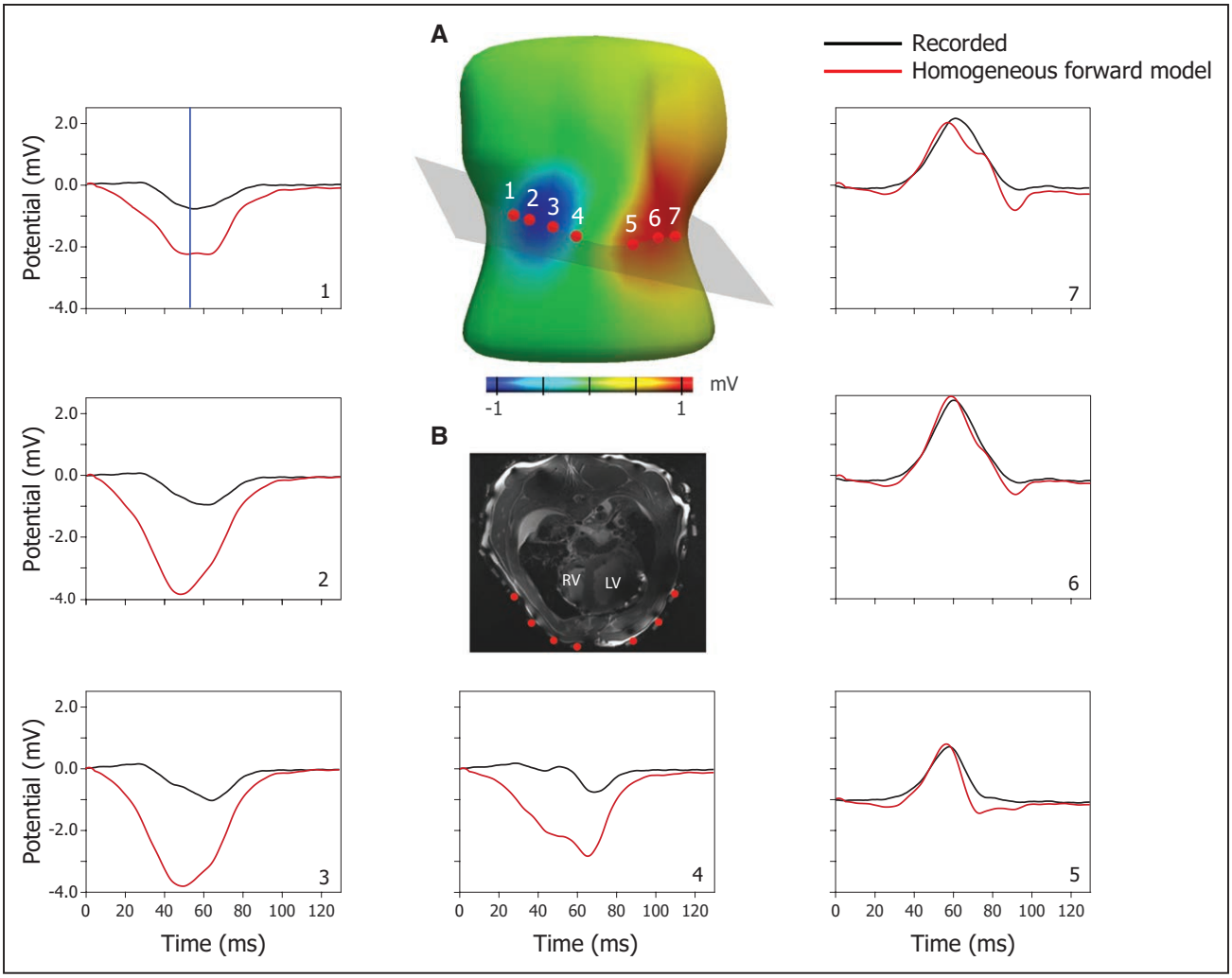

Figure 7. Comparison of precordial ECGs recorded during ventricular activation with corresponding forward reconstructions from simultaneously recorded ventricular epicardial electrograms using a homogeneous model in which torso electrical properties are assumed to uniform and isotropic. The recorded body surface potential distribution in **A** relates to the time indicated in panel 1 (blue line). Vertical projections of the electrode locations are also shown in a transverse magnetic resonance imaging cross-section in **B**, indicating the approximate locations of right ventricle (RV), left ventricle (LV), and lungs with respect to the body surface electrodes. Data from representative study in Figures 1 and 2, with epicardial pacing from the anterior RV free wall.

achieved in these studies may not be directly translatable to clinical practice.

In a previous companion study,[21] we showed that the torso does not behave as a uniform isotropic volume conductor. Measured body surface potentials were in general ≈50% of those predicted by homogeneous forward models, and the difference between them was not spatially uniform. This is illustrated in Figure 7 for the case study. Here, ECGs recorded during right ventricle pacing at sites which approximate standard precordial leads are compared with signals computed at these locations from recorded epicardial potentials, assuming homogeneous torso electrical properties. The difference between measured and predicted ECGs is much greater on the right chest (1–4) than on the left closest to the left ventricle (5–7). Large negative potentials are also reported over the right precordium when body surface potentials are simulated on the human torso in sinus rhythm using homogeneous forward models.[30] These are not seen in practice either with the 12 lead ECG or in body surface potential mapping studies.[31]

This forward error explains the 2-fold difference between measured and reconstructed epicardial RMS potentials. Furthermore, the marked regional variation of forward error on the right precordium in particular must degrade the accuracy with which epicardial electrical activity can be recovered by inverse mapping in vivo. We argue that this is the most probable reason for the significant difference in CCs for measured and reconstructed electrograms on the anterior and posterior ventricular epicardium. Our inhomogeneous forward models reduced but did not eliminate the substantial differences between predicted and recorded body surface potential maps.[21] It seems that any improvement gained from the improved forward transfer matrix has been offset by an increase in model complexity. The introduction of greater

uncertainty in organ geometries and conductivity values has, therefore, resulted in an inverse problem that is more ill posed. The mMFS performed better than F-BEM because the latter is more sensitive to geometric error but is nonetheless constrained by the fact that it is formulated with a homogeneous forward model.

Quantitative differences between our results and previous validation studies could be attributed to the inverse methods and regularization algorithms used. However, our comparisons are made with inverse solutions that use mMFS, Tikhonov regularization with a CRESO-determined regularization parameter, all methods used by previous validation studies from the Rudy laboratory,[24] and as far as we are aware, still used in their most recent studies.[32]A final observation is that there are theoretical constraints on the spatial resolution which can be achieved with inverse potential mapping.[30] Because potentials recorded on the body surface are attenuated and smoothed, they carry much less spatio-temporal information than corresponding epicardial electrograms, and the inverse problem of electrocardiography is ill posed for this reason. Stable solutions are achieved through regularization procedures that impose spatio-temporal smoothing, and this inevitably limits the extent to which complex activation and repolarization patterns can be recovered. Greater precision can be obtained by including a priori information on the nature of electrical activation in the heart.[33] However, such approaches add a further layer of electrophysiological modeling that is not applied in the inverse potential mapping that have been investigated here.

Limitations

The results presented should be considered in light of limitations inherent in the study. First, our reconstructions of torso anatomy and 3D electrode locations were based on postmortem rather than in vivo imaging. We have assumed the postmortem geometry corresponds to the static diastolic geometry. Care was taken to maintain normal lung inflation during imaging and to set cardiac filling pressures at in vivo end-diastolic levels.[21] Furthermore, MR imaging acquired in 1 pig before and after arrest confirmed that minimal error was introduced in the characterization of the epicardial geometry, with a mean distance between the postmortem and in vivo diastolic epicardial geometries of 1.3±0.8 mm.[21]

The epicardial sock used in this study and failure to restore intrathoracic pressures fully after sternotomy could alter torso electrical properties and affect body surface potentials. However, body surface potential maps recorded in a preliminary study before sternotomy and after chest closure suggest that neither the sock nor the surgery required to position it, had any material effect on body surface potential distributions (see Data Supplement in Bear et al[21]).

A potential limitation of the study is that sites of initial activation for recorded and reconstructed epicardial potentials were determined automatically. The activation maps computed provide a more robust estimate of regional activation spread than standard interpolation schemes based on the maximum negative derivative method. It is possible that an expert observer may have been able identify sites of initial activation more precisely and that LE could be overestimated as a result. However, with our approach, it was possible to analyze a relatively large data set efficiently and investigator bias was removed

Finally, evaluation of the inverse methods used in existing ECGi systems in clinical use was not performed in this study. However, we used state-of-the-art inverse solution and regularization methods and would expect the inherent accuracy of our approach to be similar to these systems.

Conclusions

Inverse potential mapping provides information on the origin and spread of epicardial activation that is useful for diagnostic screening and complements established endocardial mapping techniques. However, in our hands, the method did not recover regional epicardial electrograms reliably. In general, these were of substantially lower magnitude than recorded, and key spatio-temporal features were not reproduced. Meshless methods produced better inverse solutions than BEM and F-BEM approaches, but identification of focal epicardial activation sites was substantially worse than has been claimed previously.[5,11,12] Neither the homogeneous or the inhomogeneous models used here capture the relationship between epicardial and body surface potentials,[21] and we think that this contributes the errors identified in this study. We hypothesize that a more empirical, approach, in which regional torso conductivities are adjusted to optimize the forward transfer matrix, may provide more robust forward models.

ARTICLE INFORMATION

Received December 8, 2017; accepted March 12, 2018.

Correspondence

Laura R. Bear, PhD, IHU-LIRYC, Hôpital Xavier Arnozan, Avenue du Haut Lévêque, 33600 Pessac, France. E-mail laura.bear@ihu-liryc.fr

Affiliations

Auckland Bioengineering Institute (L.R.B., I.J.L., G.B.S., N.A.L., D.S.L., D.J.P., L.K.C., B.H.S.), Department of Physiology (I.J.L., D.S.L., D.J.P., B.H.S.), and Department of Medicine (N.A.L.), University of Auckland, New Zealand. IHU-LIRYC, Fondation Bordeaux Université, France (L.R.B.). Université de Bordeaux, France (L.R.B.). Inserm, U1045, Centre de Recherche Cardio-Thoracique de Bordeaux, France (L.R.B.). Auckland City Hospital, New Zealand (N.A.L.). Department of Physiology, Anatomy, and Genetics, University of Oxford, United Kingdom (D.J.P.).

Acknowledgments

We thank Dr Rémi Dubois for his expert opinion and Linley Nisbet for her expert technical assistance.

Sources of Funding

This study received financial support from the Health Research Council of New Zealand Programme Grant 09/067, the European grant MSCA CORDIS 3D IRSES-GA-2013-317767, the French government as part of the Investments of the Future program managed by the National Research Agency, Grant ANR-10-IAHU-04, and from the fondation Leducq through the RHYTHM transatlantic network RG 16CVD02. Dr Bear was supported by a University of Auckland Doctoral Scholarship.

Disclosures

None.

REFERENCES

1. Stevenson WG, Wilber DJ, Natale A, Jackman WM, Marchlinski FE, Talbert T, Gonzalez MD, Worley SJ, Daoud EG, Hwang C, Schuger C, Bump TE, Jazayeri M, Tomassoni GF, Kopelman HA, Soejima K, Nakagawa H; Multicenter Thermocool VT Ablation Trial Investigators. Irrigated radiofrequency catheter ablation guided by electroanatomic mapping for recurrent ventricular tachycardia after myocardial infarction: the multicenter thermocool ventricular tachycardia ablation trial. *Circulation*. 2008;118:2773–2782. doi: 10.1161/CIRCULATIONAHA.108.788604.
2. Rudy Y. Noninvasive electrocardiographic imaging of arrhythmogenic substrates in humans. *Circ Res*. 2013;112:863–874.
3. Zhang J, Desouza KA, Cuculich PS, Cooper DH, Chen J, Rudy Y. Continuous ECGI mapping of spontaneous VT initiation, continuation, and termination with antitachycardia pacing. *Heart Rhythm*. 2013;10:1244–1245. doi: 10.1016/j.hrthm.2012.01.001.
4. Sapp JL, Dawoud F, Clements JC, Horácek BM. Inverse solution mapping of epicardial potentials: quantitative comparison with epicardial contact mapping. *Circ Arrhythm Electrophysiol*. 2012;5:1001–1009. doi: 10.1161/CIRCEP.111.970160.
5. Wang Y, Cuculich PS, Zhang J, Desouza KA, Vijayakumar R, Chen J, Faddis MN, Lindsay BD, Smith TW, Rudy Y. Noninvasive electroanatomic mapping of human ventricular arrhythmias with electrocardiographic imaging. *Sci Transl Med*. 2011;3:98ra84. doi: 10.1126/scitranslmed.3002152.
6. Cuculich PS, Wang Y, Lindsay BD, Faddis MN, Schuessler RB, Damiano RJ Jr, Li L, Rudy Y. Noninvasive characterization of epicardial activation in humans with diverse atrial fibrillation patterns. *Circulation*. 2010;122:1364–1372. doi: 10.1161/CIRCULATIONAHA.110.945709.
7. Roten L, Pedersen M, Pascale P, Shah A, Eliautou S, Scherr D, Sacher F, Haïssaguerre M. Noninvasive electrocardiographic mapping for prediction of tachycardia mechanism and origin of atrial tachycardia following bilateral pulmonary transplantation. *J Cardiovasc Electrophysiol*. 2012;23:553–555. doi: 10.1111/j.1540-8167.2011.02250.x.
8. Haissaguerre M, Hocini M, Denis A, Shah AJ, Komatsu Y, Yamashita S, Daly M, Amraoui S, Zellerhoff S, Picat MQ, Quotb A, Jesel L, Lim H, Ploux S, Bordachar P, Attuel G, Meillet V, Ritter P, Derval N, Sacher F, Bernus O, Cochet H, Jais P, Dubois R. Driver domains in persistent atrial fibrillation. *Circulation*. 2014;130:530–538. doi: 10.1161/CIRCULATIONAHA.113.005421.
9. Jia P, Ramanathan C, Ghanem RN, Ryu K, Varma N, Rudy Y. Electrocardiographic imaging of cardiac resynchronization therapy in heart failure: observation of variable electrophysiologic responses. *Heart Rhythm*. 2006;3:296–310. doi: 10.1016/j.hrthm.2005.11.025.
10. Ploux S, Lumens J, Whinnett Z, Montaudon M, Strom M, Ramanathan C, Derval N, Zemmoura A, Denis A, De Guillebon M, Shah A, Hocini M, Jaïs P, Ritter P, Haïssaguerre M, Wilkoff BL, Bordachar P. Noninvasive electrocardiographic mapping to improve patient selection for cardiac resynchronization therapy: beyond QRS duration and left bundle branch block morphology. *J Am Coll Cardiol*. 2013;61:2435–2443. doi: 10.1016/j.jacc.2013.01.093.
11. Oster HS, Taccardi B, Lux RL, Ershler PR, Rudy Y. Noninvasive electrocardiographic imaging: reconstruction of epicardial potentials, electrograms, and isochrones and localization of single and multiple electrocardiac events. *Circulation*. 1997;96:1012–1024.
12. Burnes JE, Taccardi B, Ershler PR, Rudy Y. Noninvasive electrocardiogram imaging of substrate and intramural ventricular tachycardia in infarcted hearts. *J Am Coll Cardiol*. 2001;38:2071–2078.
13. Ramanathan C, Rudy Y. Electrocardiographic imaging: II. Effect of torso inhomogeneities on noninvasive reconstruction of epicardial potentials, electrograms, and isochrones. *J Cardiovasc Electrophysiol*. 2001;12:241–252.
14. Ghanem RN, Jia P, Ramanathan C, Ryu K, Markowitz A, Rudy Y. Noninvasive electrocardiographic imaging (ECGI): comparison to intraoperative mapping in patients. *Heart Rhythm*. 2005;2:339–354. doi: 10.1016/j.hrthm.2004.12.022.
15. Berger T, Fischer G, Pfeifer B, Modre R, Hanser F, Trieb T, Roithinger FX, Stuehlinger M, Pachinger O, Tilg B, Hintringer F. Single-beat noninvasive imaging of cardiac electrophysiology of ventricular pre-excitation. *J Am Coll Cardiol*. 2006;48:2045–2052. doi: 10.1016/j.jacc.2006.08.019.
16. Bhagirath P, van der Graaf M, van Dongen E, de Hooge J, van Driel V, Ramanna H, de Groot N, Götte MJ. Feasibility and accuracy of cardiac magnetic resonance imaging-based whole-heart inverse potential mapping of sinus rhythm and idiopathic ventricular foci. *J Am Heart Assoc*. 2015;4:e002222. doi: 10.1161/JAHA.115.002222.
17. Revishvili AS, Wissner E, Lebedev DS, Lemes C, Deiss S, Metzner A, Kalinin VV, Sopov OV, Labartkava EZ, Kalinin AV, Chmelevsky M, Zubarev SV, Chaykovskaya MK, Tsiklauri MG, Kuck KH. Validation of the mapping accuracy of a novel non-invasive epicardial and endocardial electrophysiology system. *Europace*. 2015;17:1282–1288. doi: 10.1093/europace/euu339.
18. Barr RC, Spach MS. Inverse calculation of QRS-T epicardial potentials from body surface potential distributions for normal and ectopic beats in the intact dog. *Circ Res*. 1978;42:661–675.
19. Cluitmans MJM, Bonizzi P, Karel JMH, Das M, Kietselaer BLJH, de Jong MMJ, Prinzen FW, Peeters RLM, Westra RL, Volders PGA. In vivo validation of electrocardiographic imaging. *JACC Clin Electrophysiol*. 2017;3:232–242. doi: 10.1016/j.jacep.2016.11.012.
20. Aras K, Good W, Tate J, Burton B, Brooks D, Coll-Font J, Doessel O, Schulze W, Potyagaylo D, Wang L, van Dam P, MacLeod R. Experimental data and geometric analysis repository-EDGAR. *J Electrocardiol*. 2015;48:975–981. doi: 10.1016/j.jelectrocard.2015.08.008.
21. Bear LR, Cheng LK, LeGrice IJ, Sands GB, Lever NA, Paterson DJ, Smaill BH. Forward problem of electrocardiography: is it solved? *Circ Arrhythm Electrophysiol*. 2015;8:677–684. doi: 10.1161/CIRCEP.114.001573.
22. Pullan AJ, Cheng LK, Nash MP, Bradley CP, Paterson DJ. Noninvasive electrical imaging of the heart: theory and model development. *Ann Biomed Eng*. 2001;29:817–836.
23. Cheng LK, Sands GB, French RL, Withy SJ, Wong SP, Legget ME, Smith WM, Pullan AJ. Rapid construction of a patient-specific torso model from 3D ultrasound for non-invasive imaging of cardiac electrophysiology. *Med Biol Eng Comput*. 2005;43:325–330.
24. Wang Y, Rudy Y. Application of the method of fundamental solutions to potential-based inverse electrocardiography. *Ann Biomed Eng*. 2006;34:1272–1288. doi: 10.1007/s10439-006-9131-7.
25. Tikhonov A, Arsenin V. *Solution of Ill-Posed Problems*. Washington, DC: John Wiley & Sons; 1977.
26. Colli-Franzone P, Guerri L, Taccardi B, Viganotti C. Finite element approximation of regularized solutions of the inverse potential problem of electrocardiography and applications to experimental data.*Calcolo*. 1985;22:91–186.
27. Duchateau J, Potse M, Dubois R. Spatially coherent activation maps for electrocardiographic imaging. *IEEE Trans Biomed Eng*. 2017;64:1149–1156. doi: 10.1109/TBME.2016.2593003.
28. Ramanathan C, Rudy Y. Electrocardiographic imaging: I. Effect of torso inhomogeneities on body surface electrocardiographic potentials. *J Cardiovasc Electrophysiol*. 2001;12:229–240.
29. Bradley CP, Pullan AJ, Hunter PJ. Effects of material properties and geometry on electrocardiographic forward simulations. *Ann Biomed Eng*. 2000;28:721–741.
30. Pullan AJ, Cheng LK, Buist ML. The forward problem. In: *Mathematically Modelling the Electrical Activity of the Heart: From Cell to Body Surface and Back Again*. Singapore: World Scientific Publishing Co. Pte. Ltd; 2005:239–326.
31. Taccardi B, Punske BB, Lux RL, MacLeod RS, Ershler PR, Dustman TJ, Vyhmeister Y. Useful lessons from body surface mapping. *J Cardiovasc Electrophysiol*. 1998;9:773–786.
32. Rudy Y. Methodology considerations and validation of electrocardiographic imaging in the Rudy laboratory. Appendix to chapter 30. In: Zipes DP, Jalife J, Stevenson WG, eds. *Cardiac Electrophysiology: From Cell to Bedside*.7th ed. Philadelphia, PA: Elsevier Health Sciences; 2017:664–667.
33. Han C, Liu Z, Zhang X, Pogwizd S, He B. Noninvasive three-dimensional cardiac activation imaging from body surface potential maps: a computational and experimental study on a rabbit model. *IEEE Trans Med Imaging*. 2008;27:1622–1630. doi: 10.1109/TMI.2008.929094.

How Accurate Is Inverse Electrocardiographic Mapping?: A Systematic In Vivo Evaluation

Laura R. Bear, Ian J. LeGrice, Gregory B. Sands, Nigel A. Lever, Denis S. Loiselle, David J. Paterson, Leo K. Cheng and Bruce H. Smaill

Circ Arrhythm Electrophysiol. 2018;11:
doi: 10.1161/CIRCEP.117.006108
Circulation: Arrhythmia and Electrophysiology is published by the American Heart Association, 7272 Greenville Avenue, Dallas, TX 75231

Print ISSN: 1941-3149. Online ISSN: 1941-3084